Research Article

Received: 27 July 2012 Revised: 14 October 2012 Accepted: 16 October 2012 Published online in Wiley Online Library: 17 December 2012

(wileyonlinelibrary.com) DOI 10.1002/jctb.3988

Preliminary studies on the electrochemical recovery of Zn and Cd from effluent produced by a zinc refinery plant using a filterpress reactor

Omar González Pérez,[a]* Sergio Castro Larragoitia[b] and Israel Rodríguez-Torres[c]

Abstract

BACKGROUND: Fundamental studies are reported investigating the electrochemical deposition of cadmium and zinc contained in solutions from a zinc electro-refining plant. This work also analyzes the performance of a filterpress electrochemical reactor used in the recovery of zinc and cadmium from this effluent.

RESULTS: The cathodic polarization curves showed electrochemical processes with mixed control for 304 SS and Al. The cyclic voltammetry studies on stainless steel revealed the presence of metal deposits at low current densities, whereas Zn and Cd were preferentially deposited at high overpotentials. The greatest recovery of cadmium (19%) and zinc (24%) at j_{ap} = 4 mA cm^{-2} was obtained with a 304 SS cathode and t = 180 min. The SEM micrographs of cathode plates confirmed the presence of cadmium and zinc deposits. In addition, EDS analyses revealed that the composition of such deposits depends on the deposition time and the cathode material.

CONCLUSION: A continuous filterpress electrochemical reactor with 304 SS and Al cathodes exhibited a promising performance level for cadmium and zinc recovery from industrial solutions.

Keywords: filterpress; electrochemical reactor; recovery; industrial effluent; wastewater treatment; zinc-cadmium

NOTATION

C^*	bulk concentration (g dm^{-3})
C_{dl}	double-layer capacitance (μF cm^{-2})
D	diffusion coefficient at infinite dilution (m^2 s^{-1})
E'	electrode potential corrected for the electrolyte ohmic resistance and referred to a saturated sulfate electrode (V)
E^0_{SSE}	thermodynamic reduction potential adjusted via the activity coefficient and referred to a saturated sulfate electrode (V)
E_{SSE}	electrode potential referred to a saturated sulfate electrode (V)
I	current (A)
j	total current density (mA cm^{-2})
j_{ap}	applied current density (mA cm^{-2})
j_C	capacitive current density (mA cm^{-2})
j_F	faradaic current density (mA cm^{-2})
j_L	limiting current density (mA cm^{-2})
j_p	peak current density (mA cm^{-2})
n_α	number of electrons involved in the rate-determining step
Q_V	volumetric flow rate (dm^3 min^{-1})
r_D	radius of disk electrode (cm)
R_S	electrolyte ohmic resistance (Ω)
S	total ionic strength (g-mole / 1000 g water)
t	time of the experiment (min or h)
T	temperature (°C)
v	potential scan rate (mV s^{-1})
X	conversion (%)
α	transfer coefficient
γ	mean ionic activity coefficient
Γ^0_S	reduced activity coefficient at the total ionic strength
κ	specific conductivity of the bulk solution (Ω^{-1} cm^{-1})
υ	kinematic viscosity of electrolyte (cm^2 s^{-1})
ω	rotation speed of the disk electrode (rpm)

* *Correspondence to: O. González Pérez, Programa de Electroquímica Aplicada e Ingeniería Electroquímica (PRELINE), Facultad de Ingeniería Química, Universidad Nacional del Litoral, Santiago del Estero 2829, S3000AOM Santa Fe, Argentina. E-mail: oglezp@fiq.unl.edu.ar*

a *Programa de Electroquímica Aplicada e Ingeniería Electroquímica (PRELINE), Facultad de Ingeniería Química, Universidad Nacional del Litoral, Santiago del Estero 2829, S3000AOM, Santa Fe, Argentina*

b *Industrial Minera México S. A. de C. V., Refinería Electrolítica de Zinc, Fracc. Morales, Domicilio conocido, 78180, San Luis Potosí, México*

c *Instituto de Metalurgia, Facultad de Ingeniería, Universidad Autónoma de San Luis Potosí, Sierra Leona 550, 78210, San Luis Potosí, México*

INTRODUCTION

The use of electrochemical reactors in the chemical industry is an alternative to common hydrometallurgical processes because of their high selectivity, as well as the high purity of the products obtained. This technology has been used in the treatment of polluting effluents and in the recovery of metals.[1–6] Electrochemical methods can be used in the electro-coating, mining, photography, battery and circuit-board industries to retrieve metals. Currently, copper, nickel, zinc, lead, cobalt, cadmium, silver and gold are the most common metals that are electrochemically recovered.

Zinc refinery plants obtain high-purity zinc through the processing, purification and electrodeposition of zinc metal. However, the presence of such impurities as sphalerite (ZnS) in the ore concentrate and their subsequent removal result in several technological and economic drawbacks. The primary impurities contained in the mineral are cobalt, nickel, cadmium, gold, silver and copper. The presence of large amounts of cadmium, silver and gold justifies the introduction of processes for the recovery of these metals because of their market value. The acid-washing stage produces two residues: cements that are sent to copper smelting and a solution that contains zinc, cadmium, cobalt and nickel, as well as other impurities. This solution is sent to cadmium refining plants, where zinc powder, zinc/cadmium cement and Sb_2O_3 are added to obtain high-purity cadmium and a waste that is subjected to a subsequent leaching step. The solution still contains cadmium, zinc, cobalt and nickel and is returned to the cadmium plant.

The recovery of metallic species from synthetic solutions has been previously studied by various authors, who have used different reactor configurations and electrode materials.[4,7–10] However, relatively little work concerning the treatment of industrial effluents has been published. The present paper aims to study the electrochemical recovery of cadmium and zinc from effluents produced by a zinc electro-refining plant using a filterpress electrochemical reactor. This study also examines the effect of time on the reactor performance. The influence of the substrates on the electrochemical separation of zinc and cadmium contained in the previously mentioned industrial effluent using synthetic solutions has been previously reported.[11] The results revealed that 304 stainless steel (304 SS) was the preferred material for the separation of Zn and Cd.

FUNDAMENTAL STUDIES WITH ROTATING DISC ELECTRODES

Experimental details

A rotating-disc electrode was used to obtain the cathodic polarization curves because this electrochemical system features well-defined hydrodynamic conditions and because the mass-transport characteristics are well-known. The working electrodes were 304 SS and aluminum discs (0.5 cm in diameter) embedded in Teflon cylinders with a diameter of 1 cm. A graphite bar with large surface area was used as a counter electrode. A saturated sulfate electrode (SSE, XR200 Radiometer Analytical) was used as a reference electrode, and all stated potentials are referred to this electrode.

The surfaces of the working electrodes were polished to a bright mirror finish with slurry of 0.05 μm alumina powder (Buehler), and the electrodes were washed with copious amounts of distilled water. To remove residual alumina, the electrodes were placed in an ultrasonic cleaner for 10 minutes. The electrodes were immersed in a 100 cm^3 glass cell, and the temperature was controlled at 25 °C using a heater–cooler (Polystat 12107–10, Cole Parmer).

The industrial effluent was an electrolyte obtained from the purification step prior to the electrolysis stage. Figure 1 shows a process diagram that illustrates the source of the sample. The effluent was filtered before the experiments to remove the suspended solids. The concentrations of cadmium, zinc, cobalt, nickel, copper and other metallic impurities were determined by atomic absorption spectroscopy (AAS, Perkin Elmer 3110). The electrolyte pH was 2.8. Prior to each experiment, the electrolyte was purged with nitrogen (Infra) for 30 min. Before the N_2 was bubbled through the electrolyte, it was deoxygenated by being passed through a pyrogallol solution.

The electrochemical measurements were performed using a potentiostat–galvanostat (Autolab PGSTAT30, Ecochemie). The cathodic polarization curves were performed on 304 SS and Al at $\omega = 0$, 100, 400, 700, 1000, 1300 and 1600 rpm and at a potential scan rate of 5 mV s^{-1}. The cyclic voltammetry studies were performed on 304 SS at 20, 40, 60, 80, 100 and 120 mV s^{-1}.

Let E' be the electrode potential corrected for the electrolyte ohmic resistance R_S:

$$E' = E - IR_S \tag{1}$$

Given that the primary current distribution represents the distribution when the surface overpotentials (activation and concentration) are neglected and when the electrode is taken as an equipotential surface, then for a disk electrode of radius r_D embedded in a large insulating plane with a counter electrode at infinity, R_S is given by:

$$R_S = \frac{1}{4\kappa r_D} \tag{2}$$

where κ is the specific conductivity of the bulk solution.[12]

The total current density is composed of faradaic (j_F) and capacitive (j_C) components:

$$j = j_F + j_C = j_F + C_{dl}\frac{dE'}{dt} \tag{3}$$

where C_{dl} is the double-layer capacitance.

Results and discussion

To correctly assign the reduction processes, it was necessary to calculate the thermodynamic reduction potential adjusted by means of the activity coefficient, which was estimated according to the method of Kusik and Meissner.[13] Table 1 shows the concentrations, activity coefficients and thermodynamic reduction potentials for all of the electroactive species, where C^* represents the bulk concentration. For $CoSO_4$, $FeSO_4$ and $PbSO_4$, the formalism of Lewis and Randall was used.[14] In the case of H_2SO_4, Staples's data[15] was used to obtain the correlation:

$$\log \Gamma_S^0 = \log\left(0.25584 + 0.01697S + 0.55328 \times 0.05258^S\right) \tag{4}$$

where S is the total ionic strength.

The γ parameter for transition metals was observed to be approximately equal for a given electrolyte and S; in this case, $\gamma \approx 0.04$. Based on E^0_{SSE} values, the deposition of aluminum and manganese can be eliminated as probable reduction processes. From a thermodynamics viewpoint, the first reduction process

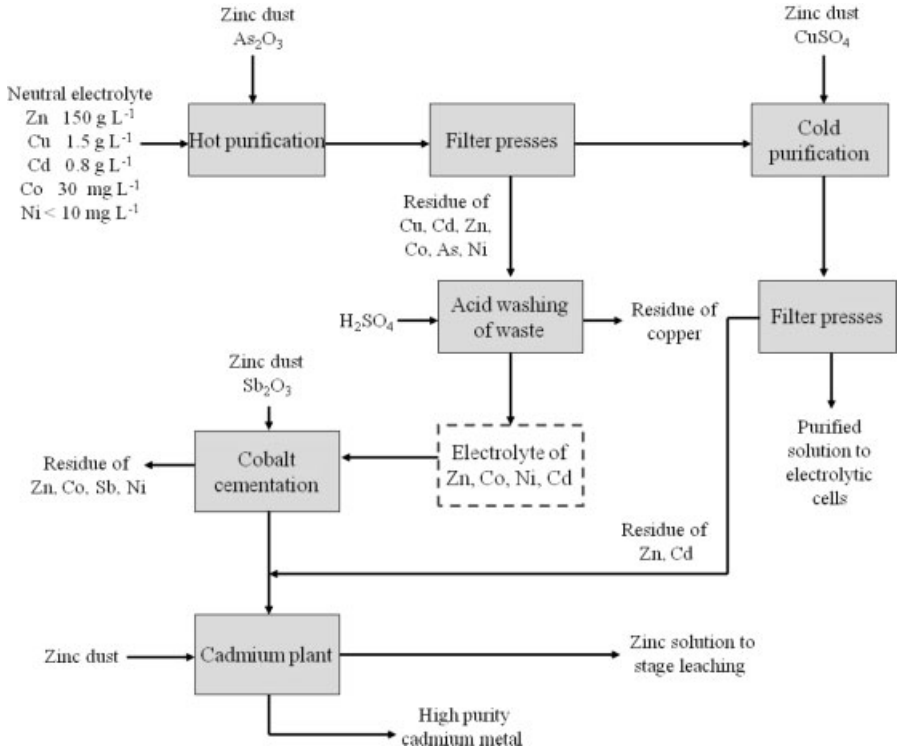

Figure 1. Process diagram showing the source of the test solution.

Table 1. Physicochemical properties and thermodynamic parameters

Species	C^* (mg dm^{-3})	$D \times 10^{10}$ (m^2 s^{-1})	$\gamma \times 10^2$	$-E^0_{SSE}$ (V)
Al^{3+}	145.6	5.41	8.547	2.392
Cd^{2+}	12283.5	7.19	4.055	1.096
Co^{2+}	841.5	7.32	4.198	0.996
Cu^{2+}	86.3	7.32	4.020	0.410
Fe^{2+}	139.5	7.19	4.593	1.181
Mn^{2+}	1276	7.12	4.331	1.893
Ni^{2+}	23.1	6.61	4.074	1.023
Pb^{2+}	6.7	9.45	2.329	0.930
Zn^{2+}	51533.5	7.03	4.129	1.431
H_2SO_4	20	93.11[a]	14.287	0.788[a]

[a] Like H^+

Table 2. Theoretical values of $-j_L$ (mA cm^{-2}) from Levich's equation at 25 °C and different ω values

ω (rpm)	Cd^{2+}	Co^{2+}	Cu^{2+}	Fe^{2+}	Ni^{2+}	Pb^{2+}	Zn^{2+}	H^+
100	33.95	4.49	0.42	0.78	0.12	0.012	241.27	3.04
400	67.91	8.98	0.84	1.55	0.23	0.024	482.55	6.08
700	89.84	11.88	1.11	2.05	0.31	0.032	638.35	8.05
1000	107.37	14.20	1.33	2.45	0.37	0.038	762.97	9.62
1300	122.42	16.19	1.51	2.80	0.42	0.044	869.92	10.96
1600	135.82	17.96	1.68	3.10	0.46	0.048	965.09	12.16

would be the deposition of copper. Subsequently, the following cathodic process would be hydrogen evolution, which would reduce the current efficiencies of Cd and Zn deposition. Later, several ions could be reduced on the working electrode surface at −1 V: Cd^{2+}, Co^{2+}, Fe^{2+}, Ni^{2+} and Pb^{2+}. Finally, zinc deposition can be performed separately or together with cadmium.

For mass-transfer-controlled systems, Levich's equation can be used to obtain theoretical values of j_L. The kinematic viscosity of the electrolyte was assumed to be 0.01 cm^2 s^{-1}. The diffusion coefficients at infinite dilution were used as an approximation.[16] The results are presented in Table 2. As in the case of activity coefficients, the D values are similar for the transition metals and are approximately 7×10^{-10} m^2 s^{-1}. Therefore, the cation concentration determines the appropriate assignation of a reduction process at a given potential. Comparatively, for $j \leq 4$ mA cm^{-2}, copper, iron, nickel and lead would exhibit mass-transfer control.

The electrical conductivity of the industrial effluent is 0.17 Ω^{-1} cm^{-1}.[17] Thus, the electrolyte ohmic resistance is 3 Ω. A typical C_{dl} value of 20 μF cm^{-2} was assumed. Figure 2 shows typical cathodic polarization curves for the industrial sample on 304 SS at 5 mV s^{-1} from stagnant electrolyte at rotation speeds of up to 1600 rpm. As shown, the curves exhibit three areas where electrochemical processes take place. The first zone, at potentials close to −0.84 V, is associated with the deposition of copper. Next, a sharp increase in current is observed at potentials near −1.12 V, which may correspond to cadmium deposition along with hydrogen evolution. The evolution of hydrogen is supported by the presence of stray signals in the polarization curves for rotation speeds greater than 100 rpm at potentials greater than −1.2 V; however, hydrogen's influence on the kinetics diminishes as the electrode rotation speed is increased. In addition, the value of the thermodynamic reduction potential of Cd^{2+} is −1.096 V. In the absence of forced convection, a peak appears at −1.18 V with a current density of −13.41 mA cm^{-2}. This peak corresponds to

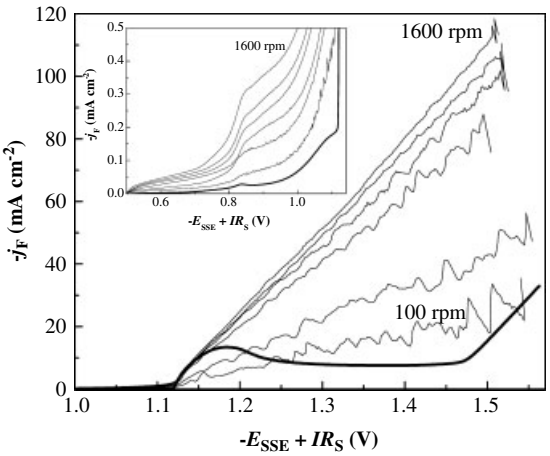

Figure 2. Current density vs. cathode potential curves for the reduction of metallic species at a 0.20 cm^2 304 stainless steel cathode. Electrolyte: N_2-purged industrial effluent. Inset: reduction processes at low current densities. Thick line: polarization curve without rotation of the working electrode. ω = 100, 400, 700, 1000, 1300, 1600 rpm. $v = 5$ mV s^{-1}, $T = 25^\circ$C.

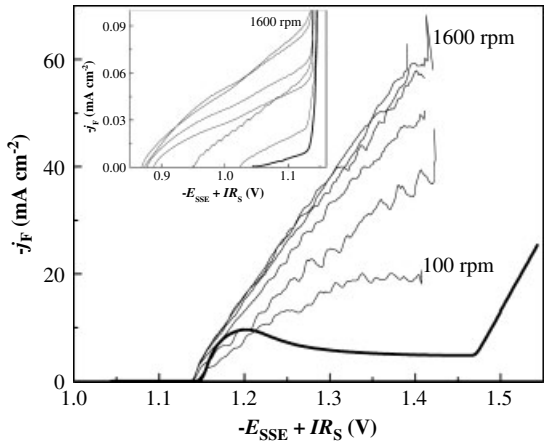

Figure 3. Current density vs. cathode potential curves for the reduction of metallic species at a 0.20 cm^2 aluminum cathode. Electrolyte: N_2-purged industrial effluent. Inset: reduction processes at low current densities. Thick line: polarization curve without rotation of the working electrode. ω = 100, 400, 700, 1000, 1300, 1600 rpm. $v = 5$ mV s^{-1}, $T = 25^\circ$C.

the cadmium electrochemical deposition process.[18] Later, a third reduction zone is observed, which is attributed to the reduction of zinc because it begins at a potential of approximately −1.47 V. This reduction potential is close to the theoretical thermodynamic value of −1.43 V. These results do not exclude the possible co-deposition of any of the other metals contained in the sample.

Because of the absence of well-defined limiting-current plateaus, the Koutecky–Levich equation could not be used to obtain kinetic parameters. An alternative method for plotting polarization curve data has been suggested by Allen and Hickling, which allows the use of data obtained at low overpotentials.[19] Assuming that the deposition of cadmium is the only electrochemical reaction at potentials between −1.1 V and −1.4 V, then $\alpha n_\alpha = 0.30$ and $j_0 = 3.05$ mA cm^{-2}.

To assign the electroactive species whose reduction results in a single peak in the polarization curve at 0 rpm, the theoretical values of peak current density for reversible and irreversible systems were calculated.[20] Based on the above values and $v = 5$ mV s^{-1}, the peak current density for the reversible deposition of cadmium would be −13.96 mA cm^{-2}, and the density of the irreversible deposition would be −5.97 mA cm^{-2}. The experimental value is located near the reversible peak current density. If the theoretical values of j_p for Zn^{2+} and H^+ are used, the calculated peak current densities are significantly greater. Therefore, it is possible to affirm that for the case of a stagnant electrolyte, the deposition of cadmium on 304 SS occurs at potentials greater than −1.1 V and that the kinetics of deposition are controlled by mass transport.

Figure 3 shows typical cathodic polarization curves for the industrial sample on aluminum at 5 mV s^{-1} from 0 up to 1600 rpm. Processes under mass-transfer control are not observed in the range of potentials analyzed. In contrast to the linear voltammograms of the stainless steel, those of the aluminum exhibit two electrochemical reduction regions. The first zone at potentials greater than −1.14 V can be associated with the deposition of cadmium. Similar to the results for 304 SS, the presence of stray signals in the system responses demonstrates that H_2 was generated on the surface of the working electrodes as the Cd^{2+} was reduced at potentials greater than −1.2 V and at low rotation speeds. Again, the curve obtained at 0 rpm exhibits a peak at −1.2 V with a current density −9.60 mA cm^{-2}. Another electrochemical process starts at a more negative potential close to −1.47 V, which is ascribed to the deposition of zinc. The potential of this peak is in good agreement with the results reported in the literature.[21] Assuming that cadmium deposition is the only electrochemical reaction for potentials between −1.1 V and −1.4 V, then $\alpha n_\alpha = 0.57$ and $j_0 = 0.35$ mA cm^{-2}. The peak current density for the reversible deposition of cadmium would be −13.96 mA cm^{-2}, whereas it would be −8.26 mA cm^{-2} in the irreversible case. Under such conditions, the experimental value would be located between the theoretical values. Therefore, we affirm that at 0 rpm, the deposition of cadmium onto Al occurs at potentials greater than −1.1 V and that the kinetics of this process are partially controlled by mass transport. Therefore, j must vary with ω; however, a plot of peak current density versus $\omega^{1/2}$ will be non-linear.

To demonstrate the processes associated with metal deposition, cyclic voltammograms were obtained using a 304 SS electrode at different sweep rates. A typical cyclic voltammogram of steel, recorded in the industrial electrolyte between the open-circuit potential (−0.4 V) and −1.4 V, is shown in Fig. 4. The main features of the voltammograms are the broad cathodic peak C3 and the corresponding anodic-stripping peak A. Two cathodic peaks (Fig. 4, bottom inset) without anodic counterparts are observed at −0.8 V (C1) and −0.9 V (C2). These processes correspond to the deposition of copper and to the adsorption of molecular hydrogen, respectively. Peak C3, located between the potentials −1.25 V and −1.34 V, corresponds to the deposition of bulk cadmium. In this potential region, the evolution of hydrogen also occurs, which is detected by direct observation and is described by the reaction:[22]

$$2H_2O_{(l)} + 2e^- \rightarrow H_{2(g)} + 2OH^-_{(aq)} \quad (5)$$

The data shown in Fig. 4 reveal that an increase in the sweep rate shifts the peak potentials to more negative values and increases the peak current.

The relationship between the cathodic peak current and $v^{1/2}$ is presented in the upper inset in Fig. 4. The variation is non-linear, and the lines do not pass through the origin. Linearity is expected for a reduction process that occurs under mass-transfer control. Processes that are reversible at low sweep rates commonly become irreversible at higher rates after having

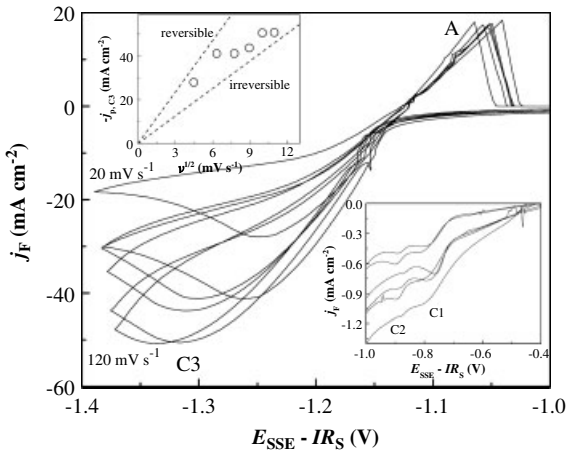

Figure 4. Cyclic voltammograms at a 0.20 cm^2 304 SS cathode. Electrolyte: N_2-purged industrial effluent. Bottom inset: reduction processes at low current densities. Upper inset:variation of the C3 peak current density as a function of the square root of the potential scan rate. $v = 20, 40, 60, 80, 100, 120$ mV s^{-1}. $\omega = 0$ rpm, $T = 25\,^{\circ}C$.

passed through a region known as the quasi-reversible region at intermediate values.[23] This transition from reversibility occurs when the relative rate of the electron transfer with respect to that of mass transport is insufficient to maintain Nernstian equilibrium at the electrode surface. In the quasi-reversible region, both the forward and reverse reactions contribute to the observed current. However, the greater-than-zero *y*-intercept values indicate that an additional process other than diffusion occurs; this behavior may be attributed to the nucleation phenomena involved.[24]

Upon sweep reversal, one current crossover appears at 80, 100 and 120 mV s^{-1}, which indicates the formation of stable growth centers at the substrate surface.[25] The mean potential value at zero current was −1.12 V. This value is more negative than that calculated from the Nernst equation (−1.096 V) because of the crystallization overpotential related to the steel substrate.[26]

The anodic stripping peak (A) centered at −1.04 V is attributed to the oxidation of metallic cadmium to Cd^{2+}. This potential is in good agreement with previously published results.[27] Usually, a metal stripping peak varies linearly with the potential scan rate; the peak's invariance in this case may be explained by the irreversibility of metal deposition and the corresponding decrease in metal deposition during the cathodic scan at high scan rates. Because the potential sweep is more positive, a sudden decrease in current is observed instead of the expected slow decline, which might suggest the formation of a non-conductive species on the substrate as a result of increased interfacial pH due to the hydrogen evolution shown in Equation (5). The precipitation of hydroxide in the cathode film is promoted by conditions that foster hydrogen evolution, which causes depletion of the hydrogen ions in the vicinity of the cathode. The pH may be several pH units higher in the cathode film than in the bulk solution, as can be seen from the formation of hydroxides in the cathode film, even at low pH levels in the bulk. The pH in the cathode film is usually higher at lower temperatures because of the slower diffusion of hydrogen ions, and in the presence of conducting salts unless the salts act as buffers.[28] Beyond peak A, the current approaches zero, which indicates that the majority of the deposited metal has been removed from the substrate surface.

Table 3. Dimensions of the electrochemical reactor

Parameter	Size
Cathode area (cm^2)	4 × 16
Anode area (cm^2)	4 × 16
Interelectrode gap (cm)	0.25
Nominal reactor volume (cm^3)	16
Hydraulic diameter (cm)	0.47

EXPERIMENTS WITH FILTERPRESS REACTOR

Experimental details

The results obtained from the electrochemical tests with the industrial effluent suggested that an electrochemical reactor with a filterpress configuration at 4 mA cm^{-2} and different operating times (3, 5 h) and different substrates (304 SS, Al) should be used. Early studies on cadmium and zinc electrowinning from acid sulfate synthetic solutions used current densities from 5 to 40 mA cm^{-2}.[29–33] However, in this work, a low current density was used because a low rate of hydrogen evolution was desired.

The reactor used is similar to a commercially available laboratory electrolyzer, the FM01-LC unit, and has an undivided configuration, as shown in Fig. 5(a). The reactor is fully described elsewhere and permits the use of a combination of spacers and gaskets compressed (by a torque wrench to a value of 25 N m) between two end plates.[34–37] The cathode configuration was a flat-plate electrode in an empty channel. The anode was a flat lead plate. The electrolyte was distributed in the filterpress reactor by internal manifolds incorporated within the cell spacers. The important cell dimensions are given in Table 3.

The flow circuit, as shown in Fig. 5(b), consisted of a 3000 cm^3 reservoir, a thermostat (12107–10, Cole Parmer Polystat), a plastic rotameter with a stainless steel float (F-44500LH-8, Blue-White Industries), two ball valves (NSF-61, Asahi Valve) and a peristaltic pump (E40513, Fasco). All interconnecting tubing was coiled piping, most of which had a 15-mm internal diameter. The flow rate was controlled in the range 2 to 6 dm^3 min^{-1}, which corresponded to calculated mean linear velocities of 33.3 to 100 cm s^{-1} in the empty channel.

The cathodes of the reactor, which were 304 SS and Al plates, were polished with emery paper (600, 1000, 1500 and 2000 grit), rinsed with distilled water, dried and weighed before and after each experiment. The anodes were trapezoidal plates of lead polished with emery paper (1000 and 2000 grit), cleaned with distilled water and dried. The initial and final values of pH were measured for each experiment.

All experiments were performed under galvanostatic control. A SSE was used as a reference electrode and was connected to a Haber–Luggin capillary positioned at the cathode plate. During the experiment, samples of solution were taken at intervals from the reactor outlet to determine the zinc and cadmium concentrations by AAS. The results obtained for the recovery of metals are expressed as the conversion as a function of time. The characterization of the deposits formed on the cathode plate at the end of the experiments was performed using scanning electron microscopy coupled with energy-dispersive X-ray spectroscopy (SEM-EDS, Philips XL30-EDAX).

Results and discussion

Table 4 summarizes the experimental conditions. The first two rows correspond to experiments with a 304 SS cathode at two different

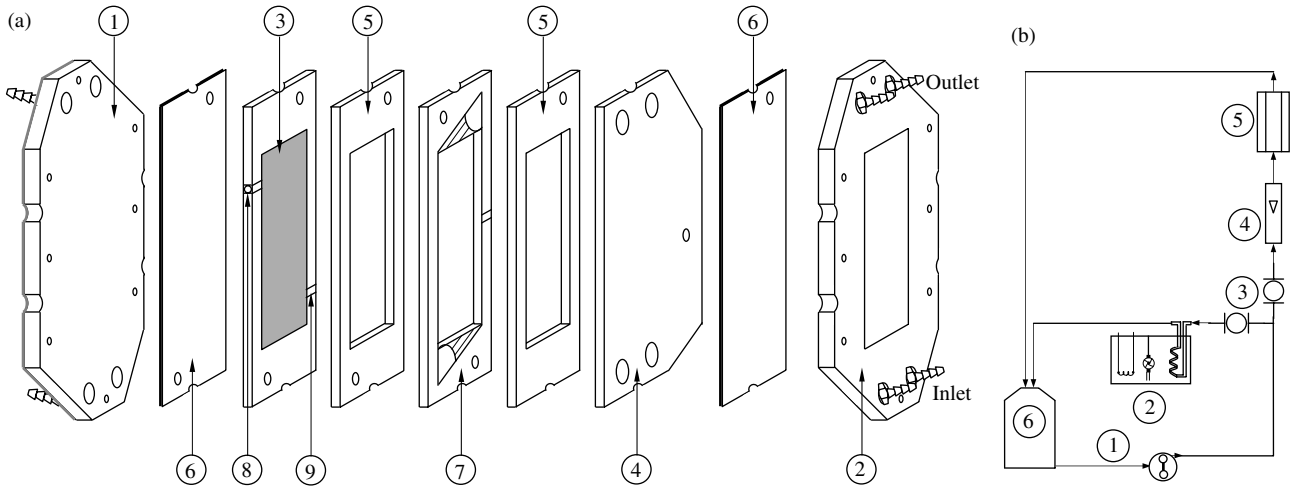

Figure 5. (a) Exploded view of the electrochemical reactor: 1, acrylic plate; 2, insulated steel backplate; 3, cathode; 4, lead electrode; 5, gaskets with central perforation; 6, polymer gaskets; 7, insulating spacer; 8, electrical connection to the cathode; 9, port for the Haber–Luggin capillary. (b) Scheme of the electrolyte circulation system:1, peristaltic pump; 2, thermostat; 3, valves; 4, flow meter; 5, electrochemical reactor; 6, reservoir.

Table 4. Summary of experimental conditions

Exp.	Cathode	I (A)	t (min)	ΔpH	$X_{Cd,\,final}$ (%)	$X_{Zn,\,final}$ (%)
1	304 SS	0.256	180	−0.65	19.29	23.65
2	304 SS	0.256	300	−1.27	14.10	21.04
3	Al	0.256	300	−1.27	20.67	6.84

operating times, 3 and 5 h, where a minor recovery of cadmium and zinc at the longer time can be attributed to peel-off, which consequently led to undesirable cadmium dissolution in the acidic electrolyte solution.[30] The experiment reported in the third row shows a higher value of cadmium recovery on aluminum compared with that on 304 SS under the same experimental conditions; however, the zinc recovery was minor. Figure 6 shows the temporal variation of cadmium and zinc fractional conversion, X, on a 304 SS cathode at $j_{ap} = 4$ mA cm^{-2}, $t = 180$ min and $Q_V = 3$ dm^3 min^{-1}. The cadmium deposition significantly increases during the first 15 min. After this time, the recovery rate remains almost constant until 140 min and reaches approximately 20% within 3 h of operation. The zinc deposition exhibits behavior similar to that of cadmium, reaching approximately 24% conversion at the end of the experiment. After this experiment, a metal foil with a thickness of 10 µm and a mass of 1.49 g was deposited uniformly along the cathode. The pH change of the effluent at the end of the experiment may indicate that the rate of oxygen evolution is greater than the rate of reduction of protons under these experimental conditions.

Under the assumption that cadmium and zinc recovery increases with reactor operating time, it was decided to use $t = 5$ h. The results obtained are illustrated in Fig. 7. As is shown, the cadmium conversion was less for $t = 5$ h compared with the previous electrolysis, yielding 14% at the end of the experiment. Zinc also exhibited a slightly decreased recovery percentage of 21%. The weight of recovered metal was 2.71 g, which is approximately twice as much as that recovered at $t = 180$ min. Likewise, a uniform deposit was obtained that was well-adhered to the steel plate.

To assess the influence on the conversion of the substrate, an aluminum cathode was used at a current density of 4 mA cm^{-2} for 5 h. The graph of the percentage conversion as a function of time

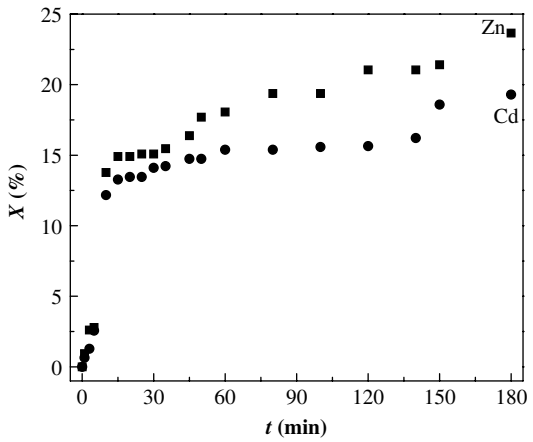

Figure 6. Conversion of cadmium (■) and zinc (●) as a function of time. Electrolyte:N_2-purged industrial effluent. Cathode:304 SS, $t = 180$ min, $Q_V = 3$ dm^3 min^{-1}, $j_{ap} = 4$ mA cm^{-2}.

is shown in Fig. 8. The results indicate an increase in cadmium recovery: 14% on stainless steel versus 21% on aluminum. The recovery of zinc was approximately one-third of that achieved with stainless steel. A powdery deposit with a mass of 2.5 g was obtained on the aluminum cathode, which is less than the mass of the foil obtained on stainless steel under the same operating conditions (j_{ap} and t), due to the lower recovery of zinc. Finally, differences in the color and texture of the products obtained using the different cathode materials may be related to the different compositions of the deposits formed on the cathode surfaces. Also, the deposit formed on the aluminum cathode was observed to have a porous appearance and poor adhesion to the cathode plate.

The surface morphology of the electrodeposits obtained from the experiments reported in Table 4 was examined by SEM, and the electron micrographs are shown in Fig. 9. Table 5 summarizes the results of the EDS analyses and the morphological features of the deposits for typical experiments. The deposits of pure cadmium from cadmium sulfate solutions on steel cathodes at low current densities are white and contain well-defined crystals.[38] The morphology of the pure zinc deposits obtained from sulfate

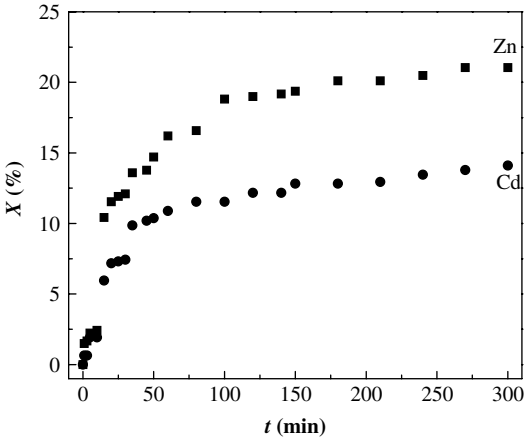

Figure 7. Conversion of cadmium (■) and zinc (●) as a function of time. Electrolyte:N_2-purged industrial effluent. Cathode:304 SS, $t = 300$ min, $Q_V = 3\ dm^3\ min^{-1}$, $j_{ap} = 4\ mA\ cm^{-2}$.

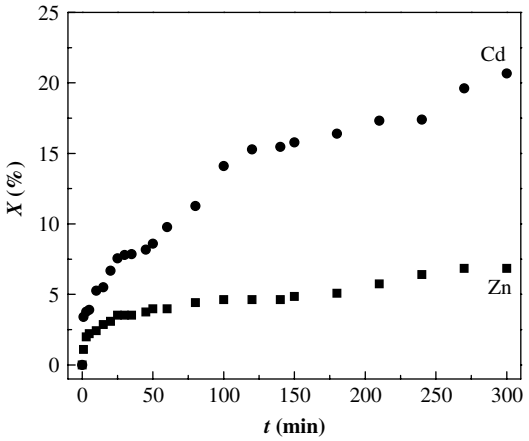

Figure 8. Conversion of cadmium (■) and zinc (●) as a function of time. Electrolyte:N_2-purged industrial effluent. Cathode:Al, $t = 300$ min, $Q_V = 3\ dm^3\ min^{-1}$, $j_{ap} = 4\ mA\ cm^{-2}$.

baths consisted of growths of parallel platelets packed together and randomly disposed.[39] The deposit obtained on 304 SS at $t = 180$ min showed island-like characteristics, as shown in Fig. 9(a), which can be attributed to the electrocrystallization phenomena on the cathode surface. Based on the spectroscopic analyses, the deposit was concluded to be composed of individual copper particles and cadmium-rich phases codeposited with zinc. When determination of the surface composition of an island was made, as shown in Fig. 9(b), the presence of two layers superimposed one above another and containing different deposits was observed: a darker region (bottom, 25Cd-Zn) and a brighter zone (upper, 69Cd-Zn). This result indicates that the process of deposition of the metallic species from the industrial effluent is more complex and is different from the plating of its individual ions.

When the operating time was increased to 5 h on a stainless steel cathode, rounded block-type structures were obtained, as shown in Fig. 9(c). In this case, the deposits were also formed by cadmium-rich phases; nevertheless, the morphology of the structures is different from that of the structures observed in the previous experiment, which can be attributed to a major deposition of cadmium. In contrast, spongy and granular deposits formed on the aluminum cathode at $t = 300$ min, as shown in Fig. 9(d). Notably, the presence of dispersed copper particles as impurities were again observed on the deposits, which were primarily composed of zinc. According to the EDS analysis, the rate of Cu deposition from the industrial effluent was similar on both cathode materials. Close inspection of the deposits obtained on Al revealed two areas of deposition, as shown in Fig. 9(e): a darker sector (located at the bottom, characterized by the presence of cobalt) and a brilliant zone located at the top. In both cases, the obtained deposits exhibited a similar composition of 61Cd-Zn.

Table 5. Summary of the morphological features and quality of the deposits shown in Fig. 9

Experiment	Morphology	at % Cd	at % Zn	at % Me
1	(a) Island-like growths	67.62	27.64	4.74[a]
	(b) Two layers of different deposits:			
	Darker region	25.23	74.77	-
	Brighter region	68.99	31.01	-
2	(c) Rounded blocks	79.21	20.79	-
3	(d) Spongy and granular structures	25.50	69.71	4.79[a]
	(e) Two layers of different deposits:			
	Darker region	57.13	39.71	3.16[b]
	Brighter region	61.89	38.11	-

[a] Copper.
[b] Cobalt.

CONCLUSIONS

1 The polarization curves showed that both 304 SS and aluminum cathodes exhibited electrochemical processes under mixed kinetic control. Also, both materials needed a similar overpotential for cadmium and zinc deposition. Furthermore, the deposition of low-concentration species on 304 SS cathodes differed from that on Al cathodes, where only cadmium and zinc deposits were obtained.

2 The cyclic voltammetry studies revealed the simultaneous deposition of metallic species present at low concentrations (copper and/or nickel and/or cobalt) together with the reduction of Cd^{2+} ions on steel electrodes. Also, hydrogen evolution was observed as a side reaction. The cadmium deposition under the studied experimental conditions exhibited mixed kinetic control. When the potential sweep was reversed, the anodic zone showed the presence of a single oxidation process with similar reaction rates for all of the investigated scan rates. This phenomenon is related to the precipitation of oxides from cadmium-rich phases, which was induced by the increased interfacial pH at the surface of the working electrode.

3 The experiments with the filterpress electrochemical reactor showed that the conversion rate decreases with increasing operating time. This decrease may be due to the re-dissolution of the cadmium and/or zinc deposits, as has been previously reported in the literature. Under the same operating conditions, the cadmium recovery was greater on aluminum, whereas the most suitable material for zinc deposition was stainless steel.

4 The morphology study of the deposits obtained on 304 SS at 180 min revealed two deposition areas with different surface

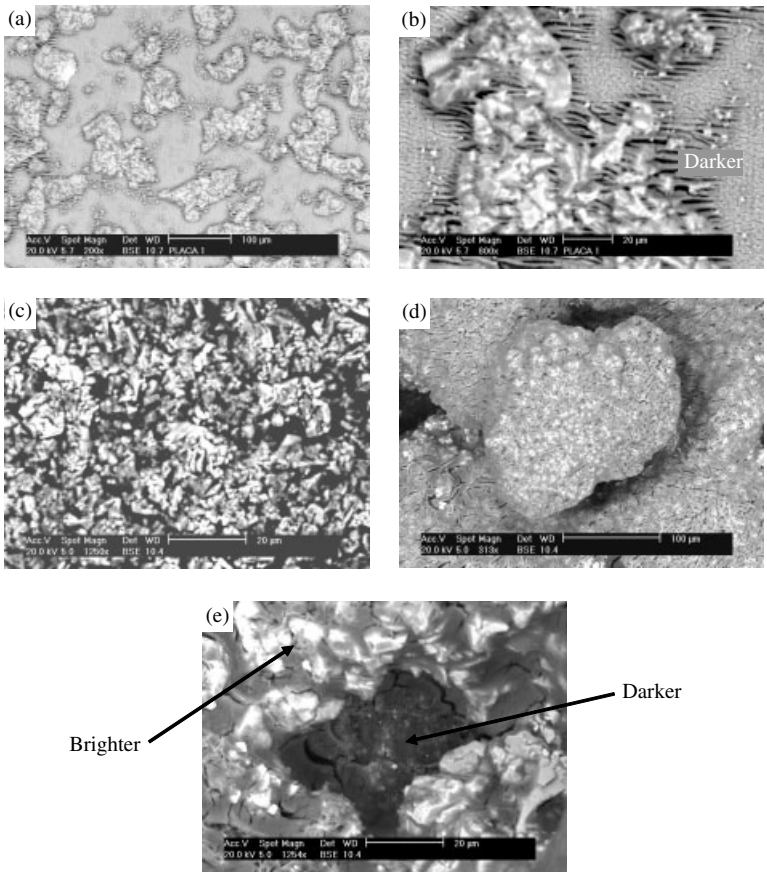

Figure 9. Scanning electron micrographs of deposits obtained from experiments reported in Table 4. Electrolyte:N_2-purged industrial effluent. $Q_V = 3\ dm^3\ min^{-1}$, $j_{ap} = 4\ mA\ cm^{-2}$, $T = 25\ ^\circ C$. (a) Cathode:304 SS, $t = 180$ min, overview; (b) cathode:304 SS, $t = 180$ min, 'island' with two layers of different deposits; (c) cathode:304 SS, $t = 300$ min, overview; (d) cathode:Al, $t = 300$ min, overview; (e) cathode:Al, $t = 300$ min, zone with two layers of different deposits.

compositions: a cadmium-rich deposit and a zinc-rich phase. For this same cathodic material and $t = 300$ min, only massive deposits with a rounded-block morphology were observed. Finally, the micrographs of an aluminum cathode revealed the presence of two distinct deposition areas with similar compositions, but they differed in that one contained individual cobalt particles or cobalt oxides precipitated on the substrate surface. Thus, the deposition of cadmium and zinc from the industrial solution is a complex process.

5 The results are promising. To improve the reactor performance, the applied current density should be increased, organic additives should be added to control the deposition rates and buffers should be incorporated to control the interfacial pH; these steps should collectively inhibit the possible precipitation of metal oxides on the cathode surface.

ACKNOWLEDGMENTS

This work was supported financially through FMSLP-2002-C01-4794 grant. OGP is thankful for the MSc (UASLP-CONACyT, México) and PhD (UNL-CONICET, Argentina) scholarships that were funded.

REFERENCES

1 Grau JM and Bisang JM, Electrochemical removal of cadmium using a batch undivided reactor with a rotating cylinder electrode. *J Chem Technol Biotechnol* **76**:161–168 (2001).
2 Mecucci A and Scott K, Leaching and electrochemical recovery of copper, lead and tin from scrap printed circuit boards. *J Chem Technol Biotechnol* **77**:449–457 (2002).
3 Rodríguez MG, Aguilar R, Soto G and Martínez SA, Modeling an electrochemical process to remove Cr(VI) from rinse-water in a stirred reactor. *J Chem Technol Biotechnol* **78**:371–376 (2003).
4 Elsherief AE, Removal of cadmium from simulated wastewaters by electrodeposition on spiral wound steel electrode. *Electrochim Acta* **48**:2667–2673 (2003).
5 Trinidad P, Walsh FC, Sheppard SA, Gillard SP and Campbell SA, The effect of operational parameters on the performance of a bipolar trickle tower reactor. *J Chem Technol Biotechnol* **79**:954–960 (2004).
6 Reade GW, Nahle AH, Bond P, Friedrich JM and Walsh FC, Removal of cupric ions from acidic sulfate solution using reticulated vitreous carbon rotating cylinder electrodes. *J Chem Technol Biotechnol* **79**:935–945 (2004).
7 St-Pierre J, Massé N, Fréchette É and Bergeron M, Zinc removal from dilute solutions using a rotating cylinder electrode reactor. *J Appl Electrochem* **26**:369–377 (1996).
8 Scott K and Paton EM, An analysis of metal recovery by electrodeposition from mixed metal ion solutions-part II. Electrodeposition of cadmium from process solutions. *Electrochim Acta* **38**:2191–2197 (1993).
9 Doulakas L, Novy K, Stucki S and Comninellis Ch, Recovery of Cu, Pb, Cd and Zn from synthetic mixture by selective electrodeposition in chloride solution. *Electrochim Acta* **46**:349–356 (2000).
10 Rodriguez-Torres I, Valentin G, Chanel S and Lapicque F, Recovery of zinc and nickel from electrogalvanisation sludges using glycine solutions. *Electrochim Acta* **46**:279–287 (2000).
11 González Pérez O, Castro Larragoitia S and Rodríguez-Torres I, Influence of the substrates on the electrochemical separation of zinc and cadmium contained in second-purification solution produced

in an electrolytic plant, in *Electrochemistry and Materials Engineering*, vol. **1**, ed by Palomar-Párdave M, Romero-Romo M, Pandalai SG and Gayathri A, Research Signpost, Kerala, Ch. 16 (2007).
12 Bard AJ and Faulkner LR, *Electrochemical Methods: Fundamentals and Applications*. John Wiley & Sons, New York (2001).
13 Kusik CL, Meissner HP, Electrolyte activity coefficients in inorganic processing. *AIChE Symp Ser* **74**:14–20 (1978).
14 Lewis GN, Randall M, The activity coefficient of strong electrolytes. *J Am Chem Soc* **43**:1112–1154 (1921).
15 Staples BR, Activity and osmotic coefficients of aqueous sulfuric acid at 298.15 K. *J Phys Chem Ref Data* **10**:779–798 (1981).
16 Vanýsek P, Ionic conductivity and diffusion at infinite dilution, in *CRC Handbook of Chemistry and Physics*, ed by Lide DR, CRC Press, Boca Raton, 5–76 (2010).
17 Aliofkhazraei M, Keshavarz Alamdari E, Zamanzade M, Salasi M, Behrouzghaemi S, Heydari J, Haghshenas DF and Vahid Zolala, Empirical equations for electrical conductivity and density of Zn, Cd and Mn sulphate solutions in the range of electrowinning and electrorefining electrolytes. *J Mater Sci* **42**:9622–9631 (2007).
18 Montiel T, Solorza O and Sánchez H, Study of cadmium electrochemical deposition in sulfate medium. *J Electrochem Soc* **147**:1031–1037 (2000).
19 Allen PL and Hickling A, Electrochemistry of sulphur. Part 1. Overpotential in the discharge of the sulphide ion. *Trans Faraday Soc* **53**:1626–1635 (1957).
20 Nicholson RS and Shain I, Theory of stationary electrode polarography. Single scan and cyclic methods applied to reversible, irreversible, and kinetic systems. *Analyt Chem* **36**:706–723 (1964).
21 Saidman SB, Muñoz AG and Bessone JB, Electrodeposition of indium and zinc on aluminium. *J Appl Electrochem* **29**:245–251 (1999).
22 Gabe DR, The role of hydrogen in metal electrodeposition processes. *J Appl Electrochem* **27**:908–915 (1997).
23 Pletcher D, Greff R, Peat R, Peter LM and Robinson J, *Instrumental Methods in Electrochemistry*. Woodhead Publishing, Cambridge (2011).
24 Trejo G, Ortega R, Meas Y, Ozil P, Chainet E and Nguyen B, Nucleation and growth of zinc from chloride concentrated solutions. *J Electrochem Soc* **145**:4090–4097 (1998).
25 Fletcher S, Halliday CS, Gates D, Westcott M, Lwin T and Nelson G, The response of some nucleation/growth processes to triangular scans of potential. *J Electroanal Chem* **159**:267–285 (1983).
26 Gomes A and da Silva Pereira MI, Zn electrodeposition in the presence of surfactants. Part I. Voltammetric and structural studies. *Electrochim Acta* **52**:863–871 (2006).
27 Jović BM, Dobrovolska Ts, Lačnjevac U, Krastev I and Jović VD, Characterization of electrodeposited Cd-Co alloy coatings by anodic linear sweep voltammetry. *Electrochim Acta* **54**:7565–7572 (2009).
28 Wranglen G, Electrodeposition of metal powders. *J Electrochem Soc* **97**:353–360 (1950).
29 Fink CG and Young CBF, Cadmium-zinc alloy plating from acid sulfate solutions. *Trans Electrochem Soc* **67**:311–338 (1935).
30 Moradkhani D, Rasouli M, Behnian D, Arjmandfar H and Ashtari P, Selective zinc alkaline leaching optimization and cadmium sponge recovery by electrowinning from cold filter cake (CFC) residue. *Hydrometallurgy* **115–116**:84–92 (2012).
31 Sadegh Safarzadeh M and Moradkhani D, The electrowinning of cadmium in the presence of zinc. *Hydrometallurgy* **105**:168–171 (2010).
32 Guillaume P, Leclerc N, Boulanger C, Lecuire JM and Lapicque F, Investigation of optimal conditions for zinc electrowinning from aqueous sulfuric acid electrolytes. *J Appl Electrochem* **37**:1237–1243 (2007).
33 Biegler T and Frazer EJ, The coulombic efficiency of zinc electrowinning in high-purity synthetic electrolytes. *J Appl Electrochem* **16**:654–662 (1986).
34 Brown CJ, Pletcher D, Walsh FC, Hammond JK and Robinson D, Studies of space-averaged mass transport in the FM01-LC laboratory electrolyser. *J Appl Electrochem* **23**:38–43 (1993).
35 Brown CJ, Pletcher D, Walsh FC, Hammond JK and Robinson D, Studies of three-dimensional electrodes in the FMO1-LC laboratory electrolyser. *J Appl Electrochem* **24**:95–106 (1994).
36 Brown CJ, Pletcher D, Walsh FC, Hammond JK and Robinson D, Local mass transport effects in the FM01 laboratory electrolyser. *J Appl Electrochem* **22**:613–619 (1992).
37 Trinidad P and Walsh FC, Hydrodynamic behaviour of the FM01-LC reactor. *Electrochim Acta* **41**:493–502 (1996).
38 Wernick S, The electrodeposition of cadmium from cadmium sulfate solutions:Part I. The effect of pH, current density, and temperature on the crystal size of the deposit, the current efficiency, and the electrode efficiency ratio. *Trans Electrochem Soc* **62**:27–38 (1932).
39 Maja M, Penazzi N, Fratesi R and Roventi G, Zinc electrocrystallization from impurity-containing sulfate baths. *J Electrochem Soc* **129**:2695–2700 (1982).

